

# No trace of a single-degenerate companion in late spectra of SNe 2011fe and 2014J.

P. Lundqvist<sup>1</sup>, A. Nyholm<sup>1</sup>, F. Taddia<sup>1</sup>, J. Sollerman<sup>1</sup>, J. Johansson<sup>2</sup>, C. Kozma<sup>1</sup>, N. Lundqvist<sup>1</sup>, C. Fransson<sup>1</sup>, P.M. Garnavich<sup>3</sup>, M. Kromer<sup>1</sup>, B.J. Shappee<sup>4</sup>, and A. Goobar<sup>2</sup>

<sup>1</sup> Department of Astronomy and The Oskar Klein Centre, AlbaNova University Center, Stockholm University, SE-106 91 Stockholm, Sweden

e-mail: peter@astro.su.se

<sup>2</sup> Physics Department and The Oskar Klein Centre, AlbaNova University Center, Stockholm University, SE 106 91 Stockholm, Sweden

<sup>3</sup> 225 Nieuwland Science, University of Notre Dame, Notre Dame, IN 46556-5670, USA

<sup>4</sup> Carnegie Observatories, 813 Santa Barbara Street, Pasadena, California 91101, USA

Received January 22, 2015; accepted ??, ??

## ABSTRACT

**Aims.** This study aims at constraining the origin of the nearby Type Ia supernovae (SNe) 2011fe and 2014J. The two most favoured scenarios to trigger the explosion of the white dwarf supernova progenitor is either mass-loss from a non-degenerate companion, or merger with another white dwarf. In the former, there could be a significant amount of left-over material from the companion at the centre of the supernova. Detecting such material would therefore favour the single-degenerate scenario.

**Methods.** The left-over material from a possible non-degenerate companion can reveal itself after about one year, and in this study such material has been searched for in spectra of SN 2011fe (at 294 days after the explosion) using the Large Binocular Telescope and for SN 2014J using the Nordic Optical Telescope (315 days past explosion). The observations are interpreted using numerical models simulating the expected line emission from ablated material from the companion star. The spectral lines sought for are H $\alpha$ , [O I]  $\lambda$ 6300 and [Ca II]  $\lambda$ 7291,7324, and the expected width of these lines is  $\sim 1000 \text{ km s}^{-1}$ , which in the case of the [Ca II] lines blend to a broader feature.

**Results.** No signs of H $\alpha$ , [O I]  $\lambda$ 6300 or [Ca II]  $\lambda$ 7291,7324 could be traced for any of the two supernovae. When systematic uncertainties are included, the limits on hydrogen-rich ablated gas in SNe 2011fe and 2014J are  $0.003 M_{\odot}$  and  $0.0085 M_{\odot}$ , respectively, where the limit for SN 2014J is the second lowest ever, and the limit for SN 2011fe is a revision of a previous limit. Limits are also put on helium-rich ablated gas, and here limits from [O I]  $\lambda$ 6300 provide the upper mass limits  $0.002 M_{\odot}$  and  $0.005 M_{\odot}$  for SNe 2011fe and 2014J, respectively. These numbers are used, in conjunction with other data, to argue that these supernovae can stem from double-degenerate systems, or from single-degenerate systems with a spun up/spun down super-Chandrasekhar white dwarf. For SN 2011fe, other types of hydrogen-rich donors can likely be ruled out, whereas for SN 2014J a main-sequence donor system with large intrinsic separation is still possible. Helium-rich donor systems cannot be ruled out for any of the two supernovae, but the expected short delay time for such progenitors makes this possibility less likely, especially for SN 2011fe. Published data for SNe 1998bu, 2000cx, 2001el, 2005am and 2005cf are used to constrain their origin. Finally, the broad lines of SNe 2011fe and 2014J are discussed, and it is found that the [Ni II]  $\lambda$ 7378 emission is redshifted by  $\sim +1300 \text{ km s}^{-1}$ , as opposed to the known blueshift of  $\sim -1100 \text{ km s}^{-1}$  for SN 2011fe. [Fe II]  $\lambda$ 7155 is also redshifted in SN 2014J. SN 2014J belongs to a minority of SNe Ia that both have a nebular redshift of [Fe II]  $\lambda$ 7155 and [Ni II]  $\lambda$ 7378, and a slow decline of the Si II  $\lambda$ 6355 absorption trough just after B-band maximum.

**Key words.** supernovae: general supernovae: individual: SN 2014J, SN 2011fe, SN 1998bu, SN 2000cx, SN 2001el, SN 2005am, SN 2005cf

## 1. Introduction

It is widely thought that a Type Ia supernova (SN Ia) is the thermonuclear explosion of a carbon/oxygen white dwarf (WD). The two most common scenarios are that the explosion could be triggered by mass transfer from a non-compact companion star (the single-degenerate scenario: Whelan & Iben 1973; Nomoto 1982), or that it is the result of a merger with another WD (the double-degenerate scenario: Whelan & Iben 1973; Iben & Tutukov 1984; Webbink 1984). While the single-degenerate (SD) scenario where a WD at the Chandrasekhar limit accretes matter from a close companion has been the most favoured scenario, there is now growing evidence that the double-degenerate (DD) scenario could be the dominant channel for SNe Ia (e.g., Maoz et al. 2014).

The lack of knowledge about the true nature of the progenitor systems of SNe Ia is a great disadvantage, since they are used as standardisable candles for distance determinations in cosmology (e.g., Goobar & Leibundgut 2011) and were used to discover the accelerating expansion of the Universe (e.g., Riess et al. 1998; Perlmutter et al. 1999). To do precision cosmology, systematic effects related to the type of progenitor system should be minimised, and possibilities to identify the nature and origin of these systems must be probed.

One way to constrain the nature of the progenitor systems is to look for merger left-over from the companion star in SD scenarios. This could either be done by searching for absorption or emission lines from a circumstellar medium (CSM) around normal SNe Ia (e.g., Mattila et al. 2005; Patat et al. 2007b; Simon

et al. 2009; Dilday et al. 2012; Lundqvist et al. 2013; Sternberg et al. 2014), or to identify material blasted off or evaporated from the non-compact companion due to the impact of the SN ejecta (e.g., Mattila et al. 2005; Leonard 2007; Shappee et al. 2013; Lundqvist et al. 2013; Maeda et al. 2014). Of these, absorption lines from a CSM may be the least conclusive, since such lines may also exist in DD scenarios (Shen et al. 2013).

Detecting early X-ray or radio emission due to interaction between the supernova ejecta and a CSM would argue for a SD scenario, but no such emission has ever been observed from a SN Ia (e.g., Panagia et al. 2006; Hughes et al. 2007; Hancock et al. 2011; Russell & Immler 2012), not even from the very nearby SNe 2011fe and 2014J, a fact that has been used to rule out most SD scenarios for those supernovae (Chomiuk et al. 2012; Margutti et al. 2012, 2014; Pérez-Torres et al. 2014). There are, however, SD scenarios predicting a very tenuous CSM in the vicinity of the explosion (e.g., Di Stefano et al. 2011; Justham 2011; Hachisu et al. 2012), so non-detections of radio and X-ray emission from SNe Ia are not necessarily fully conclusive in terms of DD or SD scenarios.

Here we concentrate on probing possible material from a SD companion in late optical spectra of SN 2014J, the closest SN Ia for decades. We do this in the same way as was previously done for six other SNe Ia (e.g., Mattila et al. 2005; Leonard 2007; Lundqvist et al. 2013; Shappee et al. 2013), including the nearby SN 2011fe. For the latter, Shappee et al. (2013) claimed an upper limit of  $0.001 M_{\odot}$  of solar-abundance material to be present in the innermost ejecta of the supernova, which is in clear conflict with hydrodynamical simulations of SD scenarios (Marietta et al. 2000; Pakmor et al. 2008; Liu et al. 2012, 2013a; Pan et al. 2012). For the other five SNe Ia, the upper mass limit was  $0.01 - 0.03 M_{\odot}$ , which is in marginal conflict with SD scenarios.

A way to avoid conflict between the lack of hydrogen lines in late spectra and hydrodynamical models is to assume that the SD companion was helium-rich. In such a case,  $0.0024 - 0.028 M_{\odot}$  (Pan et al. 2012; Liu et al. 2013b) of helium-rich material may instead pollute the innermost ejecta of the SN Ia. In Liu et al. (2013b) it was suggested to look for helium lines in this situation, but as discussed in Lundqvist et al. (2013), helium lines, due to this pollution, are not expected to be as prominent as lines of oxygen and calcium. So, in addition to look for hydrogen via  $H\alpha$ , we will here also search for oxygen and calcium lines with a width of  $\sim 1000 \text{ km s}^{-1}$ .

In our analysis, we use the same computer code to calculate the line emission from ablated mass from the SD companion as in our previous similar analyses (Mattila et al. 2005; Lundqvist et al. 2013), i.e., the model discussed in Lundqvist et al. (2013), which is based on calculations for the W7 model (Nomoto et al. 1984; Thielemann et al. 1986). Details of the modeling of late SN Ia spectra using this code for W7 are described in Sollerman et al. (2004), and in Kozma et al. (2005) for other explosion models. The results in Mattila et al. (2005) for the modelled  $H\alpha$  luminosity were extrapolated by Leonard (2007) and Shappee et al. (2013) to obtain the limits on ablated mass in those studies.

While SN 2014J is much closer to us than SN 2011fe, SN 2014J is more extinguished. One could for SN 2014J therefore expect to be about as sensitive in terms of limits on polluting mass from a SD donor, as was reported for SN 2011fe (Shappee et al. 2013). For a comparison between the two supernovae, we include them both in our analysis. Throughout the paper we adopt the distances 6.1 Mpc and 3.4 Mpc to SNe 2011fe and 2014J, respectively. For the Galactic extinction ( $R_V = 3.1$ ) we use  $E(B - V) = 0.026 \text{ mag}$  for SN 2011fe and  $E(B - V) = 0.06 \text{ mag}$  for SN 2014J. For SN 2014J we also add

$E(B - V) = 1.37 \text{ mag}$  ( $R_V = 1.4$ ) for M82. We refer to Amanullah et al. (2014), Foley et al. (2014), Goobar et al. (2014a) and Johansson et al. (2014) for a discussion on those values. For the recession velocities to the supernovae we use the host galaxy recessions, i.e.,  $+241 \pm 2 \text{ km s}^{-1}$  for SN 2011fe and  $+203 \pm 4 \text{ km s}^{-1}$  for SN 2014J (de Vaucouleurs et al. 1991). In Section 2 we describe our observations and the data, in Section 3 we show our results, and in Section 4 we provide a discussion. Finally, in Section 5 we make our conclusions.

## 2. Observations

### 2.1. Observations of SN 2011fe

SN 2011fe was observed on 2012 Jun 12.16 (JD 2456090.66), i.e., 294 days after the explosion on August 23.7, 2011, for 2 full hours with the MODS spectrograph on the 8.4-meter LBT<sup>1</sup>. The spectrum was first published by Shappee et al. (2013), and then later also by McClelland et al. (2013). We have absolute calibrated the spectrum by comparison to the  $R$ -band photometry by Munari et al. (2013). The spectrum is shown in Fig. 1.

### 2.2. Observations of SN 2014J

We observed SN 2014J with the Nordic Optical Telescope (NOT) on November 26, 2014, i.e., 315 days after the explosion on January 14.75, 2014 (Zheng et al. 2014). The NOT observations were made in service mode under NOT proposal 50-023 (P.I. A. Nyholm). The ALFOSC spectrograph was used with grism #8 and a  $1''.0$  slit (parallactic slit orientation) to get four longslit spectra with exposure time 1800 seconds per spectrum. The setup allowed us to obtain spectral coverage of the interval  $5820 - 8370 \text{ \AA}$ , where the features of interest in this investigation can be found. The expected resolution for our setup with a  $1''.0$  slit is  $\Delta\lambda = 7.0 \text{ \AA}$ . The resolution of the obtained spectra was estimated using night sky lines on each side of  $H\alpha$  in the individual spectra, and was found to be between  $7.1 \text{ \AA}$  and  $7.8 \text{ \AA}$ . At the time of the observations, there were thin clouds and variable seeing (extremes:  $0''.9$  and  $1''.3$ ). UT date for the mid-exposure time of the first and last frames was 2014 Nov 26.11 and 2014 Nov 26.17. The spectra were obtained in the airmass range  $1.43 - 1.74$ , and were reduced in the standard way with IRAF<sup>2</sup> applying overscan corrections, bias subtractions and flat fields to the individual spectra. The flat fields used were taken with the telescope pointing at the SN, directly before the SN spectra themselves were taken. A He-Ne lamp was used for the wavelength calibration and Feige 34 was used as flux standard for the four extracted, sky-subtracted SN spectra. The four individual SN spectra were then co-added. The  $R$ -band (Bessel) magnitude  $17.599 \pm 0.041$  of SN 2014J had been measured with the NOT on November 25, 2014 and this photometry was used for the absolute flux calibration of the final co-added spectrum. The co-added and flux-calibrated spectrum is shown in Fig. 1.

<sup>1</sup> The Large Binocular Telescope (LBT) and Multi-Object Dual Spectrograph (MODS; Pogge et al. 2013).

<sup>2</sup> IRAF is distributed by the National Optical Astronomy Observatories, which are operated by the Association of Universities for Research in Astronomy, Inc., under cooperative agreement with the National Science Foundation.

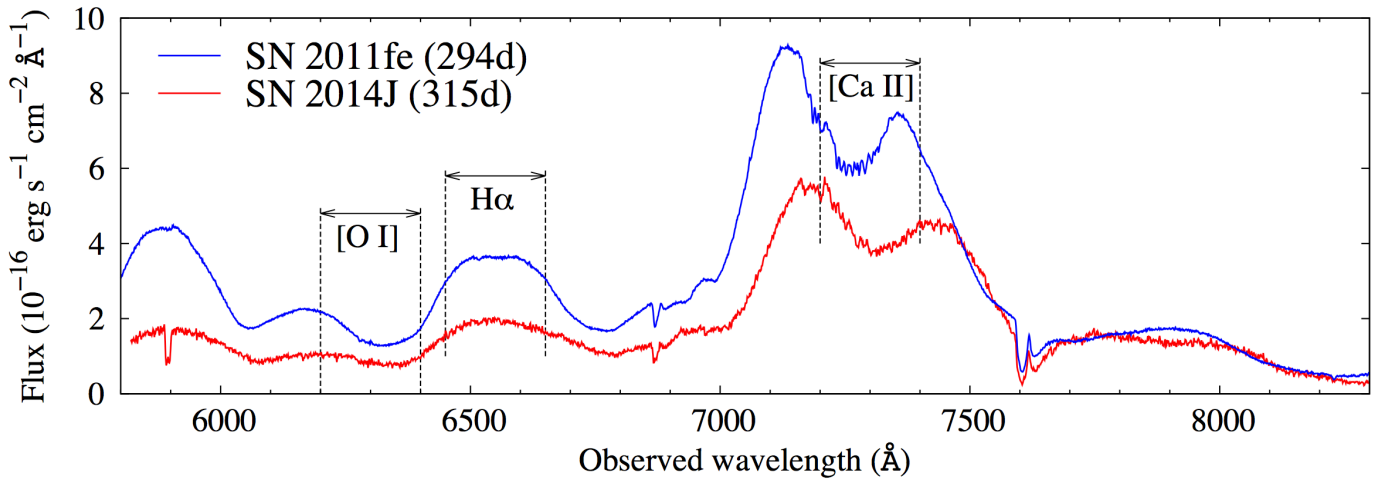


**Fig. 1.** Observed LBT spectrum (blue colour) of SN 2011fe at 294 days after the explosion (cf. Shappee et al. 2013, for the full LBT spectrum of the supernova) and observed NOT spectrum (red colour) of SN 2014J at 315 days after the explosion. No reddening or redshift correction has been made to the spectra. The recession velocities of the SNe are similar, and only  $241 \text{ km s}^{-1}$  and  $203 \text{ km s}^{-1}$ , respectively. The wavelength regions of interest for this study are marked with dashed lines and arrows. Those wavelength regions are the same as in Figs. 2 and 3. Note the general blueshift of the broad double-peak between  $7000 - 7500 \text{ Å}$  for SN 2011fe relative to SN 2014J, whereas for the peak between  $6400 - 6750 \text{ Å}$ , there is no obvious shift in wavelength. See text for further details.

### 3. Results

In Sect. 3.1 & 3.2 we discuss a strict statistical approach to estimate upper limits on the tentative line emission from the ablated gas. In Sect. 3.3 we evaluate to what extent these statistical limits can be used to really set lower limits, or whether systematic effects dominate.

#### 3.1. SN 2011fe

With the LBT spectrum we initiated our statistical approach in a similar way to what was done in Shappee et al. (2013), i.e., we smoothed the spectrum using a second-order Savitzky-Golay polynomial (Press et al. 1992). We then subtracted the non-smoothed spectrum from the smoothed one, creating a net spectrum. Like Shappee et al. (2013), we found that a smoothing width of  $\pm 30 \text{ Å}$  produced optimal net spectra.

Net spectra are shown as thin black solid lines in the left panels of Fig. 2 for the spectral regions around  $H\alpha$ ,  $[O \text{ I}] \lambda 6300$  and  $[Ca \text{ II}] \lambda \lambda 7291, 7324$ , i.e., lines that are expected from ablated gas of a SD companion (Lundqvist et al. 2013). For our further analysis, we binned the net spectra in  $10 \text{ Å}$  bins, which is also shown in these figure panels as thick black solid lines. The  $10 \text{ Å}$  binning was chosen to obtain enough number of spectral bins per expected line and to get enough number of spectral bins to study the noise within a reasonable wavelength region (see below). At the same time,  $10 \text{ Å}$  binning is fine enough to detect narrow absorption and emission features not arising in the SN.

To investigate the noise distribution of the binned net spectra in the wavelength regions of  $H\alpha$ ,  $[O \text{ I}] \lambda 6300$  and  $[Ca \text{ II}] \lambda \lambda 7291, 7324$ , we sampled fluxes in 40 wavelength bins around the wavelength of the modelled spectral lines, and compared that to the normal distribution, using a quantile-quantile test (Rice 2007). Prior to estimating the standard deviations we removed the spectral bins including the features at  $\sim 6275 \text{ Å}$  and  $\sim 6520 \text{ Å}$ , marked as telluric features by Shappee et al. (2013). In a quantile-quantile plot, a deviation from a straight line reveals a non-Gaussian distribution. As can be seen in the right

panels of Fig. 2, the noise does not deviate appreciably from that of a normal distribution, except for the  $[Ca \text{ II}]$  lines.

The estimated standard deviation, and its estimated 95% confidence level (Rice 2007), for the  $6350 - 6750 \text{ Å}$ ,  $6100 - 6500 \text{ Å}$  and  $7100 - 7500 \text{ Å}$  spectral regions are  $(6.90^{+2.10}_{-1.19}) \times 10^{-19} \text{ erg s}^{-1} \text{ cm}^{-2} \text{ Å}^{-1}$ ,  $(4.43^{+1.35}_{-0.76}) \times 10^{-19} \text{ erg s}^{-1} \text{ cm}^{-2} \text{ Å}^{-1}$  and  $(4.70^{+1.41}_{-0.80}) \times 10^{-18} \text{ erg s}^{-1} \text{ cm}^{-2} \text{ Å}^{-1}$  for each spectral region, respectively. For each spectral region, we used the maximum standard deviation within its 95% confidence level range to make a robust estimate of the  $1\sigma$  noise of the spectral bins of the expected line profiles.

Model spectra were obtained from interpolation in time, and inter- and extrapolation in ablated mass using the grid of models in Lundqvist et al. (2013) where the masses were varied between  $0.01 - 0.50 M_{\odot}$ . Extrapolation to lower masses than  $0.01 M_{\odot}$  works well for all lines considered here as collisional deexcitation of even  $[O \text{ I}] \lambda 6300$  is unimportant for such low masses. We applied appropriate redshift and reddening to the model spectra and mapped them onto the  $10 \text{ Å}$  spectral grid and created 10 000 artificial spectra by adding noise using the Monte Carlo method, where the noise was estimated from the maximum standard deviations at 95% confidence level. We ranked the simulated line fluxes, and for each line (or doublet in case of  $[Ca \text{ II}]$ ), we estimated  $1\sigma$  errors from those ranked in places 1587 and 8413. A  $3\sigma$  statistical upper limit to the ablated mass was estimated from the mass that gives a  $1\sigma$  limit of the flux that is three times lower than the modelled line flux. The left panels of Fig. 2 show the modelled line profiles (in blue) for those masses, as well as when mapped onto the spectral grid (red histogram lines). Note that for  $[O \text{ I}]$  we excluded the weak  $[O \text{ I}] \lambda 6364$  component from the analysis, as this does not add any important constraints on the oxygen mass.

For  $H\alpha$  we estimate that solar-metallicity ablated material with a mass of  $0.0010 M_{\odot}$  would have been enough to detect in the LBT spectrum. This is fully consistent with the upper limit of  $0.001 M_{\odot}$  reported by Shappee et al. (2013). For  $[O \text{ I}] \lambda 6300$  and  $[Ca \text{ II}] \lambda \lambda 7291, 7324$  we estimate that at least  $0.0023 M_{\odot}$  and  $0.0086 M_{\odot}$ , respectively, of ablated material with solar-metallicity is needed to result in a detection. These masses

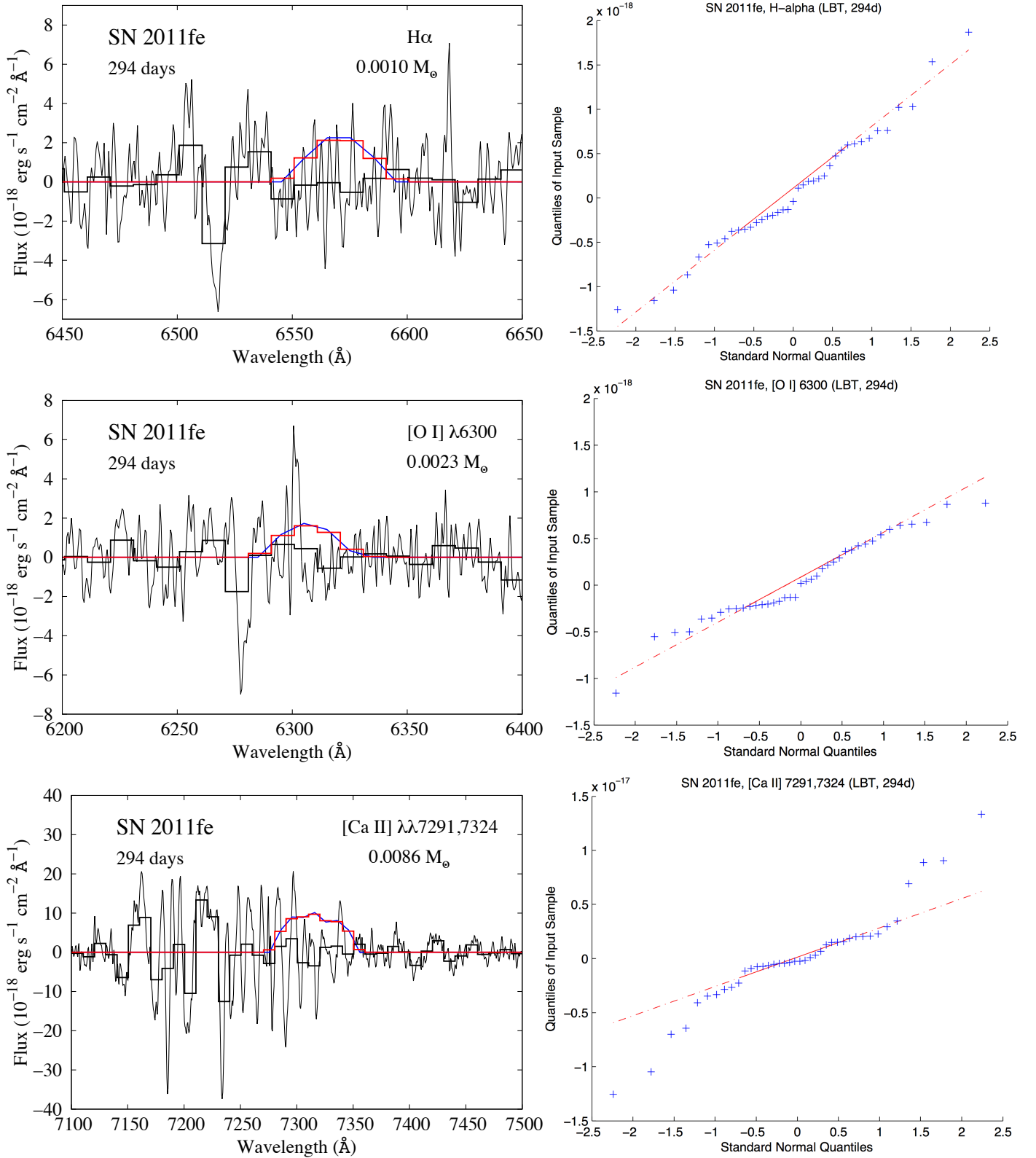


**Fig. 2.** *Left columns:* LBT net spectra (i.e., spectra after continuum removal) of SN 2011fe 294 days after the explosion (thin black lines), in the spectral regions around H $\alpha$  (upper panel), [O I]  $\lambda$ 6300 (middle panel) and [Ca II]  $\lambda\lambda$ 7291,7324 (lower panel), respectively. The thick black histogram lines show the observed spectrum after 10 Å binning. No correction for redshift was made. The blue lines show the modelled line emission, using the model in Lundqvist et al. (2013) for 294 days. The red histogram lines show the modelled flux binned to the same resolution as the binned observed spectrum. The mass of solar-metallicity material in these models are 0.0010  $M_{\odot}$ , 0.0023  $M_{\odot}$  and 0.0086  $M_{\odot}$ , respectively, and correspond to estimated  $3\sigma$  statistical upper limits of the mass. The modelled spectra have been redshifted by +203 km s $^{-1}$  and reddened by  $E(B - V) = 0.026$  mag to match the velocity and extinction of the supernova. A distance of 6.1 Mpc was used. The mass limit for H $\alpha$  agrees with that of Shappee et al. (2013) using the same data. *Right columns:* Quantile-quantile plots of the data in the net spectra. Blue data points are from the distribution of binned fluxes (in 10 Å bins) for 400 Å spectral regions around the modelled lines. The dashed red lines are for the simulated normal distribution. As can be seen, the data samples do not deviate appreciably from a normal distribution, except for the [Ca II] lines. The spectral bins dominated by telluric features at  $\sim 6275$  Å and  $\sim 6520$  Å (cf. Shappee et al. 2013) were removed from the sample prior to analysis. See text for further details.

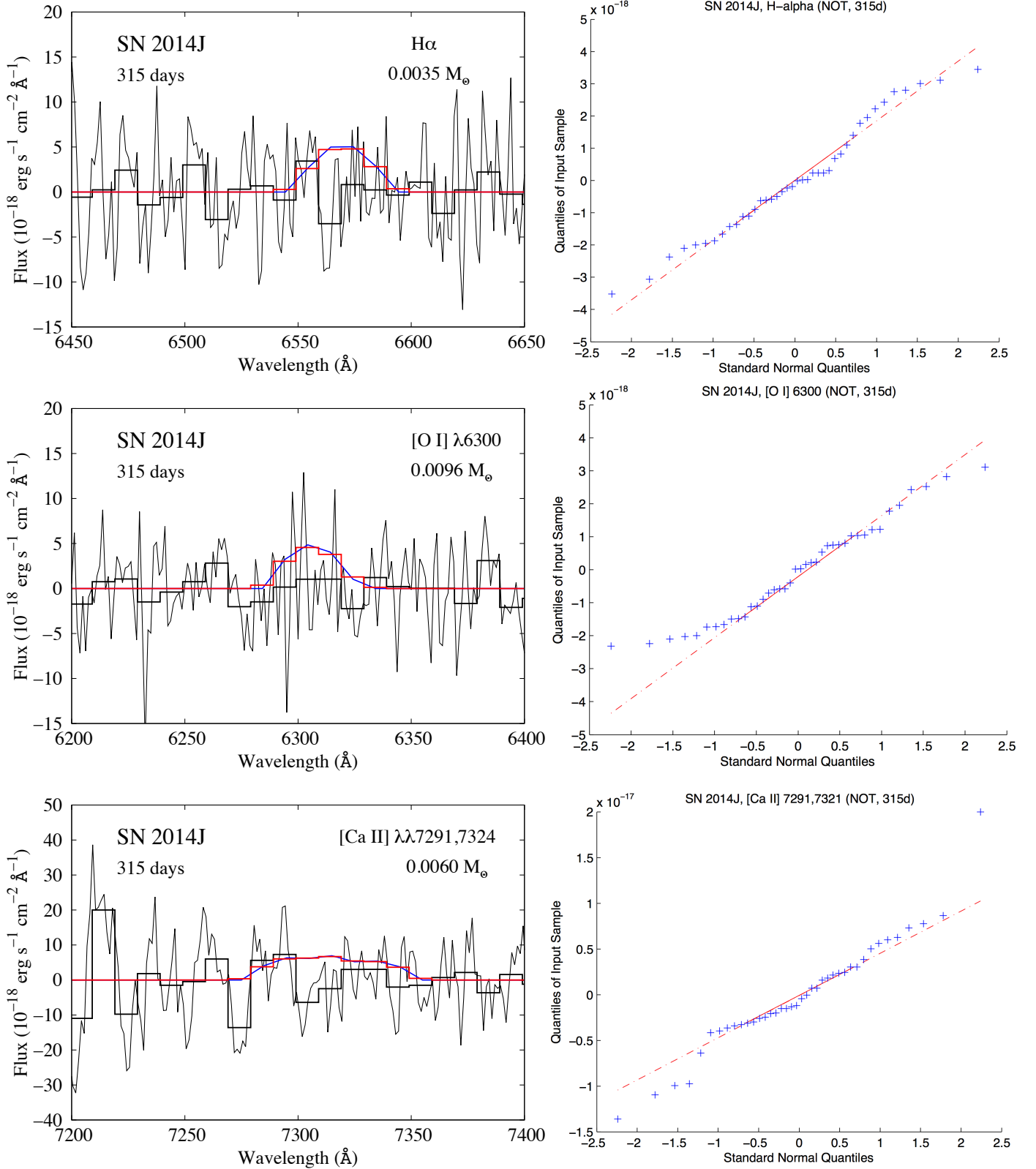


**Fig. 3.** *Left columns:* NOT net spectra (i.e., spectra after continuum removal) of SN 2014J around H $\alpha$  (upper panel), [O I]  $\lambda$ 6300 (middle panel) and [Ca II]  $\lambda\lambda$ 7291,7324 (lower panel), respectively. The thick black histogram lines show the observed spectrum after 10 Å binning. No correction for redshift was made. The blue lines show the modelled line emission, using the model in Lundqvist et al. (2013) for 315 days. The red histogram lines show the modelled flux binned to the same resolution as the binned observed spectrum. The mass of solar-metallicity material in these models are 0.0035  $M_{\odot}$ , 0.0096  $M_{\odot}$  and 0.0060  $M_{\odot}$ , respectively, and correspond to estimated  $3\sigma$  statistical upper limits of the mass. The modelled spectrum has been redshifted by +241 km s $^{-1}$  and reddened according to what is given in Section 1 to match the redshift and extinction of the supernova. A distance of 3.4 Mpc was used. *Right columns:* Quantile-quantile plots of the data in the net spectra. Blue data points are from the distribution of binned fluxes (in 10 Å bins) for 400 Å spectral regions around the modelled lines. The dashed red lines are for the simulated normal distribution. As can be seen, the data samples do not deviate appreciably from a normal distribution, except for the strongest absorption features around the [O I] line, and the strongest emission feature in the [Ca II] spectrum in the lower left panel. No spectral bins were, however, removed from the sample prior to analysis. See text for further details.

correspond to observed line fluxes of  $7.0 \times 10^{-17} \text{ erg s}^{-1} \text{ cm}^{-2}$ ,  $4.6 \times 10^{-17} \text{ erg s}^{-1} \text{ cm}^{-2}$  and  $5.5 \times 10^{-16} \text{ erg s}^{-1} \text{ cm}^{-2}$ , respectively. The relatively high limit from the [Ca II] lines is due to a noisy region in the spectrum between  $\sim 7150 - 7350 \text{ \AA}$  (cf. Fig. 1) hampered by the atmosphere.

### 3.2. SN 2014J

The NOT spectrum of SN 2014J was also smoothed using a second-order Savitzky-Golay polynomial, and from this a net spectrum was created, similar to what was done for SN 2011fe in Sect. 3.1. Again, we smoothed the spectrum with a width of  $\pm 30 \text{ \AA}$ . The net spectra for the spectral regions around H $\alpha$ , [O I]  $\lambda 6300$  and [Ca II]  $\lambda \lambda 7291, 7324$  are shown as thin black solid lines in the left panels of Fig. 3. For the further analysis, we binned the net spectra in  $10 \text{ \AA}$  bins, shown in these panels of Fig. 3 as thick black solid lines.

The noise distribution of the binned net spectra in the wavelength regions of H $\alpha$ , [O I]  $\lambda 6300$  and [Ca II]  $\lambda \lambda 7291, 7324$ , was investigated in the same way as for SN 2011fe in Sect. 3.1. The quantile-quantile plots for the noise distribution around those lines are shown in the right panels of Fig. 3. Unlike for SN 2011fe, we did not remove any outliers prior to the noise estimate. As can be seen in the right panels of Fig. 3, the noise is represented well by that of a normal distribution. There is only one obvious outlier, and that is the emission feature around  $7210 \text{ \AA}$  in the lower left panel of Fig. 3 (cf. Sect. 4.3).

The estimated standard deviation, and its estimated 95% confidence level, for the  $6350 - 6750 \text{ \AA}$ ,  $6100 - 6500 \text{ \AA}$  and  $7100 - 7500 \text{ \AA}$  spectral regions are  $(1.78^{+0.53}_{-0.30}) \times 10^{-18} \text{ erg s}^{-1} \text{ cm}^{-2} \text{ \AA}^{-1}$ ,  $(1.51^{+0.45}_{-0.26}) \times 10^{-18} \text{ erg s}^{-1} \text{ cm}^{-2} \text{ \AA}^{-1}$  and  $(6.06^{+1.82}_{-1.03}) \times 10^{-18} \text{ erg s}^{-1} \text{ cm}^{-2} \text{ \AA}^{-1}$  for each spectral region, respectively. As for SN 2011fe in Sect. 3.1, we used the maximum standard deviation within its 95% confidence level range to estimate the  $1\sigma$  statistical uncertainty for the spectral bins of the expected line profiles. Comparing the standard deviation uncertainties for SN 2014J with the  $1\sigma$  uncertainties for SN 2011fe, it can be noted that the NOT spectra are somewhat noisier than the LBT spectra in the spectral regions of H $\alpha$  and [O I]  $\lambda 6300$ , whereas the noise levels are about the same for the [Ca II]  $\lambda \lambda 7291, 7324$  spectral region. This agrees with a visual inspection of the left panels of Figs. 2 and 3.

For H $\alpha$  and [O I]  $\lambda 6300$  we estimate that solar-metallicity ablated material with a mass of  $0.0035 M_{\odot}$  and  $0.0096 M_{\odot}$ , respectively, would have been enough to detect these lines in the NOT net spectrum. These are factors of 3 – 5 higher than for SN 2011fe, mainly due to the higher extinction towards SN 2014J and the smaller telescope size of the NOT compared to the LBT. For [Ca II]  $\lambda \lambda 7291, 7324$  we estimate that at least  $0.006 M_{\odot}$  of ablated material with solar-metallicity is needed to result in a detection. This is below the limit for SN 2011fe due to modest extinction for SN 2014J in the red, as well as a noisy region of the LBT spectrum at wavelengths partly overlapping with those expected for the [Ca II] lines. The upper mass limit on ablated masses from H $\alpha$ , [O I]  $\lambda 6300$  and [Ca II]  $\lambda \lambda 7291, 7324$  correspond to observed line fluxes of  $1.6 \times 10^{-16} \text{ erg s}^{-1} \text{ cm}^{-2}$ ,  $1.3 \times 10^{-16} \text{ erg s}^{-1} \text{ cm}^{-2}$  and  $3.8 \times 10^{-16} \text{ erg s}^{-1} \text{ cm}^{-2}$ , respectively.

### 3.3. Sanity check of results

The estimated  $3\sigma$  limits on ablated mass in Sect. 3.1 and 3.2 are strictly statistical. Additional systematic errors may arise

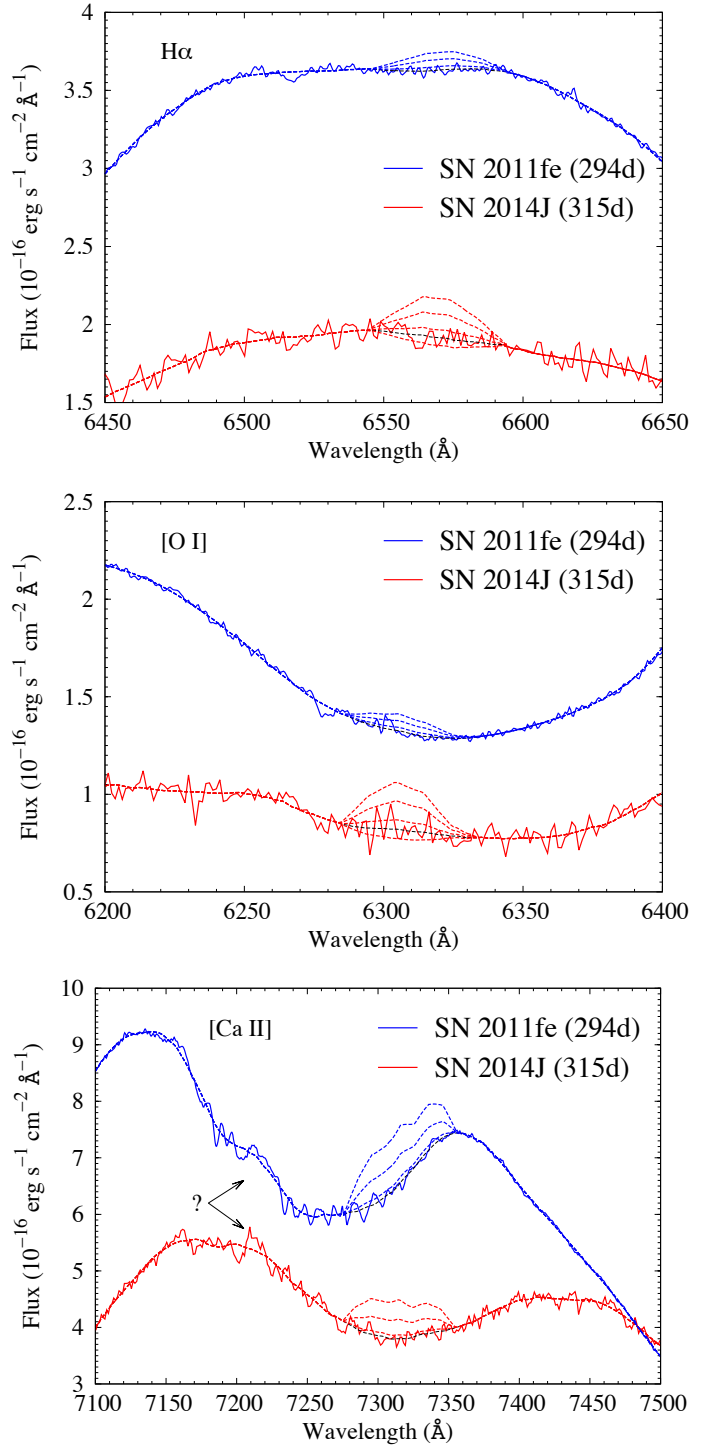


**Fig. 4.** Observed spectra (solid red and blue lines) with modelled line profiles (dashed red and blue lines) added. For H $\alpha$  (upper panel) and [O I]  $\lambda 6300$  (middle panel) the modelled fluxes are for  $1\times$ ,  $3\times$  and  $5\times$  the  $3\sigma$  statistical limits on the masses estimated in Sect. 3.1 and 3.2. For H $\alpha$  and [O I]  $\lambda 6300$  we have also subtracted  $1\times$  these masses (also shown by red dashed lines). For [Ca II]  $\lambda \lambda 7291, 7324$  (lower panel) we have added modelled fluxes corresponding to  $1\times$ ,  $5\times$  and  $10\times$  the  $3\sigma$  statistical limits on the masses estimated in Sect. 3.1 and 3.2. The dashed lines (marked in black across the line profiles) tracing the full observed spectra are the smoothed spectra using Savitzky-Golay polynomials, as outlined in Sect. 3.1 and 3.2. In the [Ca II]  $\lambda \lambda 7291, 7324$  panel, we have highlighted a feature around  $7210 \text{ \AA}$  present in the spectra of both supernovae with a question mark. Note that the plots show observed wavelengths.



due to our ignorance of the shape of the underlying spectrum from the supernova ejecta. The statistical approach artificially removes this uncertainty when the smoothed continuum is subtracted from the observed one. To highlight this, Fig. 4 shows the observed spectra, and compares that to smoothed spectra plus modelled line emission.

### 3.3.1. $H\alpha$

The upper panel of Fig. 4 shows the region around  $H\alpha$  for both supernovae. The dashed lines that strike through the spectra are from the Savitzky-Golay-smoothed continuum approximation. At the position of the line, the continuum is marked by a dashed black line. The dashed blue and red lines at that position are for  $1\times$ ,  $3\times$  and  $5\times$  the  $3\sigma$  statistical limits on the masses estimated in Sect. 3.1 and 3.2. For SN 2014J we have also added a dashed red line for a subtraction of a spectrum corresponding to the  $3\sigma$  statistical limit. An inspection by eye shows that the  $3\sigma$  statistical limit could easily be taken as part of the supernova continuum for SN 2011fe. For a clear deviation from the general shape of the continuum, one should probably require  $3\times$  the  $3\sigma$  statistical limit for SN 2011fe, and somewhat less than  $3\times 3\sigma$  for SN 2014J, to also include systematic uncertainties. This means that the limit on ablated mass from  $H\alpha$  should be  $\sim 0.003 M_{\odot}$  for SN 2011fe and  $\sim 0.0085 M_{\odot}$  for SN 2014J.

### 3.3.2. [O I] $\lambda 6300$

The middle panel of Fig. 4 shows the region around [O I]  $\lambda 6300$ . The blue, red and black lines have the same meaning as for the  $H\alpha$  panel. An inspection by eye shows that  $3\times$  the  $3\sigma$  statistical limit is probably a safe upper limit for SN 2011fe, whereas  $2\times$  the  $3\sigma$  statistical limit should certainly be enough for SN 2014J. This translates into upper limits on ablated mass using [O I]  $\lambda 6300$  to be  $\sim 0.007 M_{\odot}$  for SN 2011fe and  $\sim 0.02 M_{\odot}$  for SN 2014J.

### 3.3.3. [Ca II] $\lambda\lambda 7291, 7324$

The lower panel of Fig. 4 shows the region around [Ca II]  $\lambda\lambda 7291, 7324$  for both supernovae. Here the dashed blue and red lines at that position are for  $1\times$ ,  $5\times$  and  $10\times$  the  $3\sigma$  statistical limits on the masses estimated in Sect. 3.1 and 3.2. For SN 2011fe even more than  $5\times$  the  $3\sigma$  statistical limit produces a spectrum which mistakenly could be part of the supernova continuum bump around  $\sim 7350 \text{ \AA}$ , whereas  $5\times$  the  $3\sigma$  statistical limit probably is a fair upper limit on the ablated mass for SN 2014J. This corresponds to a limit on ablated mass from [Ca II]  $\lambda\lambda 7291, 7324$  which is  $\sim 0.06 M_{\odot}$  for SN 2011fe and  $\sim 0.03 M_{\odot}$  for SN 2014J.

## 4. Discussion

The limits on ablated mass in Sect. 3 were derived under the assumption of solar abundance composition (Anders & Grevesse 1989). This is expected in a SD scenario with hydrogen-rich gas being stripped from the companion star. However, there is also the possibility of helium-dominated gas being stripped (Pan et al. 2012; Liu et al. 2013b). If the O/He and Ca/He ratios, and the efficiency of line emission in such a scenario, do not deviate significantly from the solar composition case, our results may provide rough upper limits on the ablated mass in case of a helium-rich donor. The upper limits from [O I]  $\lambda 6300$  and

[Ca II]  $\lambda\lambda 7291, 7324$  will then be a factor of  $4([X_{\text{He}}/X_{\text{H}}]/(1 + 4(X_{\text{He}}/X_{\text{H}})))$  lower than in Sect. 3. Here  $X_{\text{He}}/X_{\text{H}}$  is the number density ratio of He and H for solar abundance. With  $X_{\text{He}}/X_{\text{H}} = 0.085$ , this factor becomes  $\approx 0.25$ , meaning that the upper limits on ablated mass from Sections 3.2.2. and 3.2.3. become  $\sim 0.002 M_{\odot}$  and  $\sim 0.005 M_{\odot}$  using [O I]  $\lambda 6300$  and  $\sim 0.015 M_{\odot}$  and  $\sim 0.008 M_{\odot}$  using [Ca II]  $\lambda\lambda 7291, 7324$  for SNe 2011fe and 2014J, respectively.

In Fig. 5 we summarise the predicted ablated masses and the upper limits from observations. We include both hydrogen- and helium-rich donors, where the predicted ablated masses for hydrogen-rich donors were taken from Pan et al. (2012) and those expected in the helium-rich case from Pan et al. (2012) and Liu et al. (2013b). For the results of Pan et al. (2012), we have used the information in their Table 2, while for the results of Liu et al. (2012, 2013b) we follow the advice in Liu et al. (2013b) to assume that 50% of the gas lost from the companion due to supernova impact is ablated. The mass range of ablated hydrogen-rich gas is therefore  $0.052 - 0.091 M_{\odot}$  according to Liu et al. (2012, which supersedes the models of Pakmor et al. 2008) or  $0.0139 - 0.636 M_{\odot}$  according to Pan et al. (2012), while for the helium-rich case, we have in Fig. 5 marked the ranges  $0.00245 - 0.0134 M_{\odot}$  (Pan et al. 2012) and  $0.0095 - 0.028 M_{\odot}$  (Liu et al. 2013b).

Our limits are sensitive to the velocity of the stripped/ablated gas. We have assumed that the ablated gas is confined to  $10^3 \text{ km s}^{-1}$ . This assumption agrees with the results of Pan et al. (2012), where the peak of the velocity distribution is well below  $10^3 \text{ km s}^{-1}$  for hydrogen-rich donors, but just short of this velocity for helium-rich donors (see also Liu et al. 2013b, for a confirmation); there is a significant fraction of gas with velocities in the range  $(1 - 2) \times 10^3 \text{ km s}^{-1}$  in the helium-donor case. A higher velocity than our assumed  $10^3 \text{ km s}^{-1}$  results in shallower emission line profiles from the ablated gas, and the limits on ablated gas for helium-rich donors should therefore be shifted upwards in Fig. 5. Judging from the velocity distribution of the ablated gas in Pan et al. (2012), the upward shift could be a factor of  $\sim 1.3 - 1.5$ , whereas for hydrogen-rich donors the factor could instead be shifted in the other direction by a similar amount since the expected velocity of the ablated gas is well below  $10^3 \text{ km s}^{-1}$  for such donors.

## 4.1. Implications for SNe 2011fe and 2014J

### 4.1.1. Constraints from our findings

From Fig. 5 it is obvious that hydrogen-rich donor stars are disfavoured for both SNe 2011fe and 2014J. Pan et al. (2012) made models for both red giant and main sequence companions, and the main sequence stars populate the lower part of the range marked ‘Liu12’ in Fig. 5. Red giant hydrogen-rich companions for SNe 2011fe and 2014J are therefore clearly ruled out in terms of ablated mass. The models with the lowest amount of ablated gas are those with main-sequence companions, and among these the ablated mass decreases with increasing orbital separation. The largest separation tested by Pan et al. (2012) was  $2.75 \times 10^{11} \text{ cm}$ , corresponding to  $5R_{\star}$ , where  $R_{\star}$  is the donor star radius. They found a power-law relation between the separation (in units of  $R_{\star}$ ) and the amount of unbound matter from the donor. Extrapolating their grid of models, the separation would need to be  $\geq 6 R_{\star}$  for the ablated mass to be as low as our upper limit for SN 2014J, and  $\geq 8.5 R_{\star}$  for SN 2011fe. Models with such large separation were tested by Pakmor et al. (2008), who found that the stripped mass could be below  $0.01 M_{\odot}$  for models

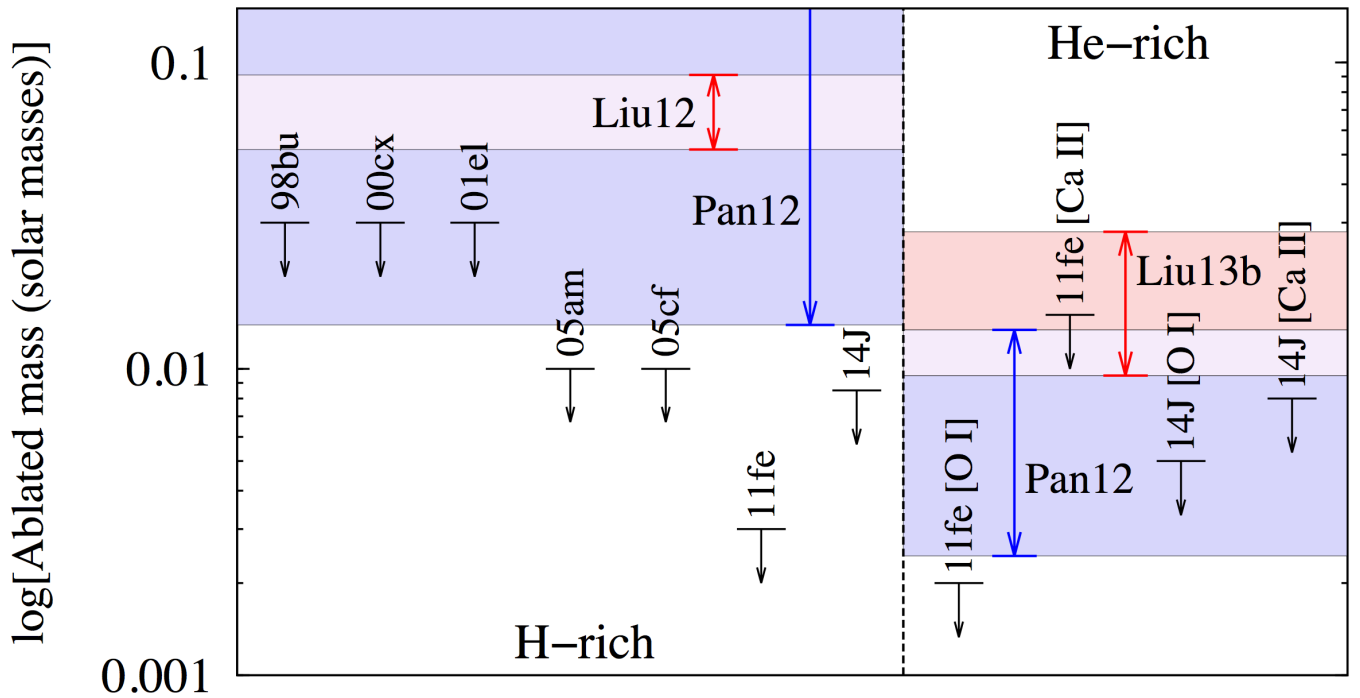


**Fig. 5.** Summary of estimated upper limits on the mass of ablated gas from a SD companion. The estimates for SNe 1998bu and 2000cx are from Lundqvist et al. (2013), the one for SN 2001el from Mattila et al. (2005), the ones for SNe 2005am and 2005cf from Leonard (2007), and the ones for SNe 2011fe and 2014J are from this paper. The left part of the figure is for hydrogen-rich gas, and the right part is for helium-dominated gas. Simulated ranges of ablated mass are marked by filled areas and arrows. For hydrogen-rich donors, red is for Liu et al. (2012) and blue is for Pan et al. (2012), while for helium-dominated donors, red is for Liu et al. (2013b) and blue is for Pan et al. (2012). Note that our limits for both SNe 2011fe and 2014J are below the simulated ranges for hydrogen-rich gas, while helium-rich donors cannot be fully ruled out, in particular not for SN 2014J, if we are guided by the simulations of Pan et al. (2012). See text for further details.

with large separation, and even lower if the explosion energy is reduced. Although the trends are clear, the exact numbers in Pakmor et al. (2008) are uncertain, as cautioned by Liu et al. (2012) and Pan et al. (2012).

While the models explored by Pan et al. (2012) used binary evolution models of Ivanova & Taam (2004) as input, Liu et al. (2012) modelled both the binary evolution and simulated the explosion impact themselves. Liu et al. (2012) concentrated on main sequence companions, and, like Pan et al. (2012), they found a clear trend of decreasing ablated mass for increasing binary separation when expressed in  $R_*$ . The ablated mass is, however, larger than in the models of Pan et al. (2012), and our mass limits on ablated hydrogen-rich gas for both SNe 2011fe and 2014J are much lower than in the models of Liu et al. (2012). It remains to be tested which of the impact simulations are the most accurate in terms of ablated mass. In any case, a large separation is necessary to make the impact models compatible with our limits on ablated hydrogen-rich gas.

If the SD companion were instead a helium-rich donor, the right part of Fig. 5 shows that it is only our limits for SN 2011fe which are below the expected mass of ablated gas from impact models. However, if one adjusts for a likely slightly larger velocity of the ablated gas for helium-rich donors than assumed in the construction of Fig. 5, we cannot rule out all models of helium-rich donors in Pan et al. (2012) even for SN 2011fe. For SN 2014J, our upper limits from both [O I]  $\lambda 6300$  and [Ca II]  $\lambda \lambda 7291, 7324$  are higher than the lower part of the range of ablated masses in the models of Pan et al. (2012). Like for the hydrogen-rich case, it is the systems with the largest separation that produce the least amount of helium-rich ablated gas in

these models. The helium-rich companion in Pan et al. (2012) is from Wang et al. (2009), and not from simulations of binary evolution. There could therefore be some uncertainty regarding the binary evolution, and thus perhaps the amount of ablated gas. Liu et al. (2012), on the other hand, follow the detailed binary evolution leading up to the explosion. The smallest amount of unbound material from the companion occurs for the systems with the largest separation. Like for hydrogen-rich companions, there is an inconsistency between the impact models of Liu and co-workers and Pan et al. (2012) with regard to the amount of ablated mass. Until this is settled, it cannot be ruled out that the progenitor system of SN 2014J, and perhaps even that of SN 2011fe, could have been a WD with a helium-rich non-degenerate companion at large separation.

#### 4.1.2. Checking against other constraints on SNe 2011fe and 2014J

Pre-explosion imaging of SN 2011fe (Li et al. 2011) cannot fully rule out a helium-rich donor as a possibility for the origin of the system. Donors with  $M_V \gtrsim -0.6$  mag, in combination with  $T_{\text{eff}} \gtrsim 50\,000$  K are allowed. Here  $M_V$  is the absolute visual magnitude of the donor at the time of explosion. Using the bolometric corrections of Torres (2010), the bolometric luminosity of a tentative helium-rich donor in the SN 2011fe progenitor system was  $\log(L_{\text{bol}}/L_{\odot, \text{bol}}) \lesssim 3.5$ . Most of the helium-donor stars in Liu et al. (2013b), and Wang et al. (2009, who made a thorough investigation of helium-donor systems) have properties in this range, so our analysis (cf. Fig. 5) could be more constraining than the pre-explosion imaging, especially if the impact models of Liu et



al. (2013b) are closer to the real situation than those of Pan et al. (2012) in terms of ablated gas.

Related to our results for SN 2011fe is the *Swift* study by Brown et al. (2012). The non-detection of very early ultraviolet emission from the supernova limits the parameter space of allowed SD companions to only include main-sequence companions with masses  $\lesssim 2 - 3.5 M_{\odot}$ , and perhaps even  $\lesssim 1 M_{\odot}$ , for close companions. Geometric probabilities are less than 1% for a  $2 (1) M_{\odot}$  main-sequence star separated from the white dwarf by  $5(3) \times 10^{11}$  cm, i.e., close to the largest separation of  $3 \times 10^{11}$  cm tested by Pan et al. (2012) for hydrogen-rich companions, and decreases further for larger separation. Our analysis for SN 2011fe, in combination with the models of Pan et al. (2012) rules out a SD system with a hydrogen-rich donor at a separation of  $\lesssim 8.5 R_{\star} \sim 4 \times 10^{11}$  cm. Adding the constraints from the analysis of the *Swift* observations essentially rules out all SD scenarios with a main-sequence hydrogen-rich donor for SN 2011fe. A  $2 - 3 M_{\odot}$  main-sequence could be possible if it lies within a few degrees along the line-of-sight on the rear side of the white dwarf. Such a star would also pass the limits set by the pre-explosion imaging (Li et al. 2011), but is likely at odds with the very early optical observations discussed by Bloom et al. (2012).

The only hydrogen-rich SD scenario reasonably possible for SN 2011fe is that of a spun up/spun down super-Chandrasekhar WD (Di Stefano et al. 2011; Justham 2011; Hachisu et al. 2012). In such systems the donor star shrinks far inside its Roche lobe prior to the explosion, making the SD companion smaller and more tightly bound. The supernova ejecta impact on such a star should also produce low enough emission to pass the limits from the early UV observations of Brown et al. (2012). Furthermore, very small amounts of ablated gas are expected, as well as very dilute ( $n \sim 1 \text{ cm}^{-3}$ ) circumstellar gas in the vicinity of the supernova. A way to constrain this scenario is through continued deep monitoring of the supernova in radio (Pérez-Torres et al. 2014).

Our results for SN 2011fe are also consistent with previous findings (cf. Maoz et al. 2014) that it may indeed have been the outcome of a DD scenario. What speaks in favour of a DD scenario rather than the spun up/spun down super-Chandrasekhar WD scenario is that SN 2011fe was a normal SN Ia in terms of lightcurve and spectral evolution, and that the spun up/spun down super-Chandrasekhar WD scenario is not thought to be the normal path leading to a SN Ia explosion. However, while the DD scenario for SN 2011fe may be likely, we cannot rule out a spun up/spun down super-Chandrasekhar WD. Neither can we fully rule out a helium-rich donor at large separation (cf. above). Using the numbers in Fig. 5 and figure 12 in Pan et al. (2012), we estimate that we cannot rule separations which are  $\gtrsim 6 R_{\star} \sim 8 \times 10^{10}$  cm and  $\gtrsim 4.5 R_{\star} \sim 6 \times 10^{10}$  cm for helium-rich donors for SNe 2011fe and 2014J, respectively. Even if not explicitly discussed by Brown et al. (2012), helium-rich donor systems with such small separation may not be well constrained by the early *Swift* observations of SN 2011fe.

Recently, Taubenberger et al. (2014) reported very late (1034 days past explosion) observations of SN 2011fe. No sign of narrow H $\alpha$  was found, but this could be due to poor signal-to-noise. A tentative identification of [O I] was, however, made, which would make SN 2011fe the third SN Ia ever, besides SNe 1937C (Minkowski 1939) and the subluminal 2010lp (Taubenberger et al. 2013), to show signs of [O I] in late spectra. The [O I] emission in SN 2010lp is unlike that we expect from ablated gas since the line profiles indicate emission at velocities offset by  $\sim 1900 \text{ km s}^{-1}$  from the rest wavelengths of [O I]  $\lambda\lambda 6300, 6364$ . If the [O I] identification is correct for SN 2011fe, then a simi-

larly large offset ( $\sim +2000 \text{ km s}^{-1}$ ) would apply. The [O I] emission in these SNe has therefore probably nothing to do with ablated gas from a companion, but should come from blobs of oxygen-rich SN ejecta. In the case of SN 2011fe, we emphasise that the [O I] identification could also be a misinterpretation, as the emission may very well be due iron (Taubenberger et al. 2014).

Just as for SN 2011fe, the progenitor system for SN 2014J, could have been a DD system, a spun-up/spun-down super-Chandrasekhar WD scenario, or a system with a helium-rich companion at large separation. For SN 2014J, our results could also be compatible with a well-separated hydrogen-rich donor system. A recent clue, perhaps in favour of a SD scenario, was the reported early variation in two narrow absorption components of K I  $\lambda 7665$  (Graham et al. 2014). The estimated distance from the supernova to the absorbing gas is, however,  $\sim 10^{19}$  cm, which is  $\sim 50 - 100$  times further away from the supernova than the likely position of a circumstellar blast wave after 1 year (Pérez-Torres et al. 2014). Continued monitoring in radio may pick up circumstellar gas closer to the supernova. Unlike narrow absorption lines, radio is sensitive to any gas close to the supernova, and not only gas along the line of sight to it.

Further clues to the origin of SN 2014J come from very early photometry of the supernova. As reported by Goobar et al. (2014b), the rise in luminosity during the first few days after explosion indicates an extra energy source which could be due to interaction of the ejecta with a non-degenerate companion (cf. Kasen 2010) or the debris from a disrupted WD (e.g., Levanon et al. 2014). The matter interacting with the ejecta must be confined to the immediate vicinity of the explosion site since radio observations only 8 – 9 days after the explosion did not reveal any emission (Chandler & Marvil 2014, see also Pérez-Torres et al. 2014).

Analysis of pre-explosion images (Kelly et al. 2014) shows that a DD progenitor system, a helium-star donor with low effective temperature ( $T_{\text{eff}}$ ), or a system like U Sco (recurrent nova and a supersoft-X-ray source with a subgiant companion) would not show up in the pre-explosion images. On the other hand, SD systems like V445 Pup (bright helium-star donor) or RS Oph (bright recurrent nova and a symbiotic source) are both excluded.

More specifically, the pre-explosion imaging of SN 2014J cannot rule out helium-star donors with  $M_V \gtrsim -2.5$  mag in combination with  $T_{\text{eff}} \gtrsim 40\,000 \text{ K}$  (cf. Figure 4 of Kelly et al. 2014). Again, using the bolometric corrections of Torres (2010), the bolometric luminosity of a tentative helium-rich donor in the SN 2014J progenitor system was  $\log(L_{\text{bol}}/L_{\odot, \text{bol}}) \lesssim 4.4$ . The helium-donor stars in Liu et al. (2013b) and Wang et al. (2009) all have properties in this range, so our analysis (cf. Fig. 5) is more constraining than the pre-imaging for helium-donor stars, in particular if the simulations of Liu et al. (2013b) are more representative than those of Pan et al. (2012). We note, however, that Liu et al. (2013b) assume that the metal abundance of the helium-rich donor remains at  $Z = 0.02$  (i.e., the solar value) even when hydrogen has been removed, whereas we have in Fig. 5 assumed that this number is a factor of 4 higher for helium-rich donor compared to hydrogen-rich ones. If we abandon this correction factor, and also consider the slightly larger velocity of the ablated gas in the helium-rich scenario than assumed in Fig. 5, the ablated mass in the models of Liu et al. (2013b) become consistent with our results, in particular for the helium-star donors with the largest separation to the WD. Removing the correction factor of 4 could make it easier to accommodate a helium-star donor system also for SN 2011fe. For SN 2014J, we note that a

helium-rich donor was argued for by Diehl et al. (2014) to explain the early emergence of gamma-ray line emission.

#### 4.2. Broad lines of SN 2011fe and 2014J

The main spectral peak between 7050–7250 Å for SN 2014J is centered at  $\approx 7170$  Å, whereas it is shifted to the blue at  $\approx 7135$  Å for SN 2011fe. This is close to the rest-wavelength of [Fe II]  $\lambda 7155$ . Likewise, the main peak between 7250–7300 Å and 7500 Å is clearly shifted more to the blue for SN 2011fe, where the peak occurs at  $\sim 7355$  Å, compared to  $\sim 7420$  Å for SN 2014J. Most of this peak can be attributed to [Ni II]  $\lambda 7378$ . Correcting for the redshifts of the SNe, and assuming that [Fe II]  $\lambda 7155$  and [Ni II]  $\lambda 7378$  are the main contributors (see also Maeda et al. 2010b; Taubenberger et al. 2014; Graham et al. 2015), the [Fe II]  $\lambda 7155$  peak occurs at  $\sim -1000$  km s $^{-1}$  and  $\sim +400$  km s $^{-1}$  for SNe 2011fe and 2014J, respectively, whereas for [Ni II]  $\lambda 7378$  they are at  $\sim -1100$  km s $^{-1}$  and  $\sim +1300$  km s $^{-1}$  for SNe 2011fe and 2014J, respectively. There is thus a consistent blueshift for SN 2011fe, which is in full agreement with McClelland et al. (2013, see also Graham et al. 2015), whereas the lines are redshifted for SN 2014J. Figure 1 does not show any obvious similar shifts between the supernovae for the broad peaks with centers around 5900 Å and 6550 Å, which are thought to be dominated by [Co III] lines (Maeda et al. 2010b; Taubenberger et al. 2014; Graham et al. 2015). This is in agreement with the analysis of Maeda et al. (2010b) where [Fe II]  $\lambda 7155$  and [Ni II]  $\lambda 7378$  mainly originate from the dense central parts of the ejecta where asymmetries can be expected, as opposed to the more highly ionized exterior region, which is closer to being spherically symmetric. Maeda et al. (2010b) argue that this is a natural outcome of a delayed-detonation scenario, and exemplify this for 12 SNe Ia. Half of them have shifts of [Ni II]  $\lambda 7378$  in excess of 1500 km s $^{-1}$ . Both SNe 2011fe and 2014J have smaller velocity offsets, which may just be a viewing angle effect.

Maeda et al. (2010a) further connect the viewing angle to how fast the absorption trough of Si II  $\lambda 6355$  recedes after *B*-band maximum. The decline rate in this velocity ( $v_{\text{SiII}}$ ) is called  $\dot{v}_{\text{Si}}$ , and Maeda et al. (2010a) argue that SNe Ia with  $\dot{v}_{\text{Si}} \gtrsim 70$  km s $^{-1}$  d $^{-1}$  (the so-called high-velocity gradient, or HVG, group, cf. Benetti et al. 2005) all have redshifted [Fe II]  $\lambda 7155$  and [Ni II]  $\lambda 7378$  emission in nebular spectra. There is also a small fraction of those SNe Ia with  $\dot{v}_{\text{Si}} \lesssim 70$  km s $^{-1}$  d $^{-1}$  (the so-called low-velocity gradient, or LVG, group) that have redshifted nebular lines, but the majority of the LVG group SNe Ia have blueshifted [Fe II]  $\lambda 7155$  and [Ni II]  $\lambda 7378$  emission.

Consulting the results of Kawabata et al. (2014) and Marion et al. (2015) for SN 2014J, we find that  $\dot{v}_{\text{Si}} \sim 55$  km s $^{-1}$  d $^{-1}$  (between 0 – 30 days after *B* maximum) and  $\dot{v}_{\text{Si}} \sim 50$  km s $^{-1}$  d $^{-1}$  (between –0.7 and +9.3 days after *B* maximum), respectively. Furthermore, Ashall et al. (2014) found  $\dot{v}_{\text{Si}} \approx 58.8$  km s $^{-1}$  d $^{-1}$  between 0 – 10 days after *B* maximum using their observations. This would put SN 2014J in the LVG group, and the supernova would belong to the minority of SNe Ia which are both LVG group objects and have redshifted nebular [Fe II]  $\lambda 7155$  and [Ni II]  $\lambda 7378$  emission. Another one in this category is SN 2001el (Maeda et al. 2010a, this SN is further discussed in Sect. 4.4). We note that no LVG SNe in Benetti et al. (2005) have  $v_{\text{SiII}} \geq 11000$  km s $^{-1}$  around *B*-band maximum, whereas  $v_{\text{SiII}} \approx 11750$  km s $^{-1}$  for SN 2014J at that epoch (Ashall et al. 2014; Kawabata et al. 2014; Marion et al. 2015).

For the LVG group SN 2011fe (Parrent et al. 2012; Graham et al. 2015), the blueshifted nebular [Fe II]  $\lambda 7155$  and [Ni II]  $\lambda 7378$  emission fits well into the model of Maeda et al. (2010a, see also McClelland et al. 2013). SN 2011fe had also notably lower  $v_{\text{SiII}}$  than SN 2014J around *B*-band maximum (Parrent et al. 2012; Goobar et al. 2014a).

#### 4.3. The 7210 Å feature in the spectra of SN 2011fe and 2014J

As indicated in Fig. 4, there appears to be a spectral feature around the observed wavelength 7210 Å for both SN 2011fe and 2014J, with a width roughly like that expected from a single spectral line from ablated gas. Had this feature coincided with the expected wavelength of, e.g., H $\alpha$ , the flux of the feature would have corresponded to a level greater than the  $3\sigma$  statistical limit of the H $\alpha$  flux in Fig. 3, and could have mistakenly been taken as evidence of ablated gas. This shows the importance of making a sanity check like that in Sect. 3.3, and not just relying on statistical errors to set upper limits on spectral line fluxes. The question arises whether the feature is due to clumpiness/asymmetry in the supernova ejecta, ablated gas from a companion, some other source, or if it is an observational artefact. The feature is seen in all four individual frames for SN 2014J and appears in both SNe. From an inspection of Fig. 1, the feature appears to be the only one of its sort, except perhaps for a feature at 7155 Å in the SN 2014J spectrum. The spectra of SN 2011fe at 329 days by Graham et al. (2015) and at 331 days by Taubenberger et al. (2014) have, unfortunately, too low signal-to-noise to support or reject the tentative feature at 7210 Å for that SN.

We have used The Atomic Line List V2.05B18<sup>3</sup> to search for possible spectral lines that could explain the 7210 Å feature of both SNe in Fig. 4, but find no obvious counterpart other than those most likely responsible for the main peaks, i.e., the usual suspects of forbidden lines of Fe and Ni (e.g., McClelland et al. 2013). Neither do we find any other obvious candidate for the 7155 Å feature. We have also looked at late spectra of SNe 1998bu, 2000cx, 2001el and 2005cf (cf. Fig. 5 for references discussing these spectra), but do not find a similar feature for those SNe. This could partly be due to lower signal-to-noise in the spectra of these SNe. In any case, there is no support for a 7210 Å feature in their spectra.

The 7155 Å and 7210 Å features occur in a spectral region with telluric molecular absorption, which can also be traced in the standard stars used during the LBT and NOT runs. The most likely explanation for the features is that they are therefore observational artefacts from this absorption.

#### 4.4. Implications for SNe 1998bu, 2000cx, 2001el, 2005am and 2005cf

Apart from SNe 2011fe and 2014J, Fig. 5 shows upper limits on hydrogen-rich ablated gas for the five previous SNe Ia for which there are upper limits on H $\alpha$  in late spectra. These limits are all lower than in the models of Liu et al. (2012), and are also close to the lowest mass of hydrogen-rich ablated gas in the models of Pan et al. (2012). No estimated limits on helium-rich ablated gas exist for these SNe. Possible progenitor models for these five SNe could therefore be helium-rich donor systems, DD systems, spun-up/spun-down super-Chandrasekhar WD progenitors, or perhaps hydrogen-rich donor systems with a large separation be-

<sup>3</sup> <http://www.pa.uky.edu/~peter/newpage/>

tween the WD and the non-degenerate companion, likely being a main-sequence star as donor (cf. the models of Pan et al. 2012). The only systems fully ruled out are those with red giant donors, and those with close main-sequence donors. According to figure 12 of Pan et al. (2012), main-sequence donor systems with a separation of  $\lesssim 6R_*$  are ruled out for SNe 2005am and 2005cf, as well as  $\lesssim 4.5R_*$  for SNe 1998bu, 2000cx, 2001el.

There are limited constraints on the progenitor systems of these supernovae from other investigations. For example, narrow emission lines were looked for in spectra of SNe 2000cx and 2001el, but no such emission was detected (Mattila et al. 2005; Lundqvist et al. 2013), and SN 2000cx showed no time-varying narrow interstellar/circumstellar absorption features (Patat et al. 2007a). SN 1998bu had a light echo (Cappellaro et al. 2001; Garnavich et al. 2001), but that was due to foreground material, and not to circumstellar matter. SN 2005cf was observed early in the ultraviolet (UV) with the *HST* (Wang et al. 2012) and with *Swift*, starting  $-8.8$  and  $-7.8$  days before  $B$  maximum, respectively. A comprehensive compilation of data and an analysis were presented in Gall et al. (2012), but there is no evidence of enhanced early flux indicative of the ejecta interacting with nearby material. *Swift* also observed SN 2005am in the UV from  $-1$  day, and onwards (Bufano et al. 2009), but nothing conspicuous with regard to the nature of the progenitor system was detected.

Among all these SNe, SN 2000cx is clearly the oddball. Although it shares some properties with the overluminous SN 1991T, it is different enough to form a separate category together with SN 2013bh (Silverman et al. 2013). It probably stems from an old, low-metallicity population, which together with its spectral evolution indicate a DD or a SD delayed detonation scenario (Silverman et al. 2013, and references therein). As a helium-star donor system is likely to originate from relatively massive progenitors, Wang et al. (2009) estimate that the maximum delay time for these SNe is  $\sim 10^8$  years. This probably rules out such a progenitor for SN 2000cx.

#### 4.5. Uncertainties

In our models we have used the W7 model (Nomoto et al. 1984) which produces  $0.6 M_\odot$  of  $^{56}\text{Ni}$ . The excitation of the ablated gas depends on the exact amount of  $^{56}\text{Ni}$ , as well as the distributions of the nickel and the ablated gas. It also depends on where the positrons deposit their energy. As discussed in Sollerman et al. (2004), we have assumed local and instantaneous deposition of the positron energy. Neither microscopic nor macroscopic mixing of the ablated gas into the supernova ejecta was made. How all this is included and treated in our models affects the predicted fluxes of the lines we discuss. However, none of these uncertainties should translate into dramatic changes with regard to the modelled line emission.

Of potentially greater importance is the fact that the number of elements and atomic levels in our models are somewhat limited (cf. Sollerman et al. 2004, and references therein). This could make us underestimate line scattering and fluorescence. As noted in Pérez-Torres et al. (2014), more recent models (e.g., Jerkstrand et al. 2011) with more extensive line lists and more complete sets of ions and atomic levels, albeit not yet time-dependent, should be used to estimate these effects.

As we have remarked, the amount of ablated gas, or rather, the gas lost by a SD companion at velocities  $\lesssim 10^3 \text{ km s}^{-1}$  after impact differs between models from different research groups. This is highlighted by Fig. 5. Further such modelling is warranted. In particular for the fairly restricted range of possible progenitor systems of SNe 2011fe and 2014J (cf. Sect. 4.1).

As an important boundary condition for possible SD progenitor systems, one must consider the strengthened evidence of a fairly long ( $10^8$  yrs) minimum delay time for SNe Ia in general (e.g., Anderson et al. 2014). This could prove hazardous for the helium-star donor channel since the maximum delay time for such systems could be  $\sim 10^8$  yrs (Wang et al. 2009). Refined binary evolution models are needed to see whether this channel is likely to produce a noticeable fraction of SNe Ia.

There is also uncertainty in our results due to the adopted distance and reddening to the supernovae. According to NED<sup>4</sup>, the uncertainty in distance to SN 2011fe is  $\sim 6\%$  and for modern measurements to M82 (for SN 2014J) it is  $\sim 9\%$ . If we assign  $10\%$  as an uncertainty for the distance in general, this transforms into  $\sim 20\%$  in estimated values for the ablated mass. For SN 2011fe, uncertainties due to reddening is not an issue, whereas for SN 2014J the reddening is significant. There is good knowledge about the absolute luminosity so the reddening is well established (Amanullah et al. 2014). The combined effect of distance and reddening is estimated to cause an uncertainty in the ablated mass of  $\sim 30\%$  for SN 2014J. This is not insignificant, but smaller than the uncertainties in our modelling.

## 5. Conclusions and outlook

We have observed SN 2014J with NOT/ALFOSC at 315 days after the explosion, and also used an archival spectrum of SN 2011fe 294 days past explosion (presented in Shappee et al. 2013) to see if there is any trace of ablated gas from a SD companion. Guided by our modelling in Lundqvist et al. (2013), we have concentrated on possible emission in H $\alpha$ , [O I]  $\lambda 6300$  or [Ca II]  $\lambda \lambda 7291, 7324$ . We find no such emission, and from that we derive statistical upper limits on the mass of hydrogen-rich gas. These limits are, however, shown to be overwhelmed by systematic effects. When the latter are included, the limits on hydrogen-rich ablated gas are  $0.003 M_\odot$  and  $0.0085 M_\odot$  for SNe 2011fe and 2014J, respectively, where the limit for SN 2011fe should supersede that of Shappee et al. (2013), and that for SN 2014J is the second lowest ever. Assuming that the O/He and Ca/He ratios, and the efficiency of line emission, are the same for helium-dominated ablated gas and for hydrogen-rich gas, we derive upper limits on the mass of helium-rich ablated gas. In this case, [O I]  $\lambda 6300$  provides the most stringent upper limits on the ablated gas, which are  $0.002 M_\odot$  and  $0.005 M_\odot$  for SNe 2011fe and 2014J, respectively.

These upper limits are compared with the most recent models predicting the amount of stripped and ablated gas presented by Liu et al. (2012, 2013b) and Pan et al. (2012). For hydrogen-rich donors, our results are incompatible with red giants, and with main-sequence donors if the separation between the binary companions are  $\lesssim 6 R_*$  for SN 2014J and  $\lesssim 8.5 R_*$  for SN 2011fe, where  $R_* = 5.51 \times 10^{10} \text{ cm}$  is the radius of the main-sequence companion in the models of Pan et al. (2012). Also, most helium-rich donors are ruled out, except for those with the largest separation. Using the models of Pan et al. (2012), helium-rich donors with a separation of  $\lesssim 8 \times 10^{10} \text{ cm}$  and  $\lesssim 6 \times 10^{10} \text{ cm}$  from the white dwarf are ruled out for SNe 2011fe and 2014J, respectively.

When we combine these results with findings from pre-explosion imaging and very early observations constraining possible interactions with a companion, accretion disk or circumstellar matter, then essentially all hydrogen-rich main-sequence

<sup>4</sup> <http://ned.ipac.caltech.edu>

donor systems can be ruled out for SN 2011fe, while we cannot state this for SN 2014J. For both supernovae, our results are the most constraining so far for helium-rich donors. Helium-rich donor systems may, however, have other problems, since the likely modelled delay time of such systems is  $\lesssim 10^8$  years (Wang et al. 2009), at the same time as recent observational findings of SNe Ia show a general delay time of  $\gtrsim 10^8$  years (Anderson et al. 2014), leaving only a low probability of these systems to be progenitors of SNe Ia in general. Some support for a single-degenerate origin of SN 2014J could come from very early observations showing enhanced emission compared to the expected one (Goobar et al. 2014b) for an isolated exploding white dwarf, as well as the early emergence of gamma-ray line emission (Diehl et al. 2014). According to our findings, the tentative non-degenerate companion would have to be well separated from the white dwarf. Other possible progenitor systems for SNe 2011fe and 2014J are single-degenerate systems with a spun up/spun down super-Chandrasekhar white dwarf, or double-degenerate systems. Continued radio monitoring of the SNe may reveal if any of these systems could be possible (Pérez-Torres et al. 2014).

Data for SNe 1998bu, 2000cx, 2001el, 2005am and 2005cf are used to constrain their origin. Possible progenitor models for these SNe are found to be helium-rich donor systems, DD systems, spun-up/spun-down super-Chandrasekhar WD progenitors, or perhaps systems with a main-sequence star as donor, provided they are well separated from the white dwarfs. However, as for SNe 2011fe and 2014J, helium-rich donors could be rather unlikely due to their short delay times, and is probably excluded for SN 2000cx due to the nature of its host galaxy.

For the broad lines of SNe 2011fe and 2014J it is found that the [Ni II]  $\lambda 7378$  emission is redshifted by  $\sim +1300$  km s $^{-1}$ , as opposed to a blueshift of  $\sim -1100$  km s $^{-1}$  for SN 2011fe. Also, [Fe II]  $\lambda 7155$  appears to be redshifted for SN 2014J, and it has distinct substructures. Broad lines at shorter wavelengths, and dominated by [Co III] line emission, do not show velocity shifts between SNe 2011fe and 2014J. This fits nicely into the model of Maeda et al. (2010b), where low-ionisation lines are expected from asymmetrically distributed matter in the centre, whereas higher-ionisation lines originate further out where spherical symmetry is more likely. Both SNe 2011fe and 2014J have a slow decline rate of the velocity of the Si II  $\lambda 6355$  absorption trough just after  $B$ -band maximum. SN 2011fe fits well into the general picture that such supernovae have blueshifted nebular emission, while SN 2014J belong to a minority which instead have redshifted nebular emission. SN 2014J also has a larger velocity ( $\approx 11750$  km s $^{-1}$ ) of this trough at  $B$ -band maximum than usual.

Although we cannot count on being blessed with more very nearby SNe Ia like SNe 2011fe and 2014J in the near future, late spectra have now been obtained for more than just a handful SNe. As shown in Fig. 5, useful constraints on progenitor systems can be put on SNe Ia also at 20 – 30 Mpc, using our method. Concerted multi-wavelength efforts should be able to narrow down possible progenitor systems of SNe Ia. Both very early observations in order to constrain/detect possible interaction with a binary or circumstellar gas, as well as late observations in the optical/infrared to constrain emission from ablated gas and in radio to map circumstellar/interstellar gas, are needed.

**Acknowledgements.** We thank Jussi Harmanen, Tapio Pursimo and Ditte Slumstrup for making the spectroscopic observations at the NOT, and Rahman Amanullah for discussions. PL acknowledges support from the Swedish Research Council. This research has made use of the NASA/IPAC Extragalactic Database (NED) which is operated by the Jet Propulsion Laboratory, California Institute

of Technology, under contract with the National Aeronautics and Space Administration.

## References

- Amanullah, R., Goobar, A., Johansson, J., et al. 2014, *ApJ*, 788, L21  
 Anders, E., & Grevesse, N. 1989, *Geochim. Cosmochim. Acta*, 53, 197  
 Anderson, J. P., James, P. A., Förster, F., et al. 2014, *MNRAS*, accepted [arXiv:1412.6315]  
 Ashall, C., Mazzali, P., Bersier, D., et al. 2014, *MNRAS*, 445, 4424  
 Benetti, S., Cappellaro, E., Mazzali, P. A., et al. 2005, *ApJ*, 623, 1011  
 Bloom, J. S., Kasen, D., Shen, K. J., et al. 2012, *ApJ*, 744, L17  
 Brown, P. J., Dawson, K. S., de Pasquale, M., et al. 2012, *ApJ*, 753, 22  
 Bufano, F., Immler, S., Turatto, M., et al. 2009, *ApJ*, 700, 1456  
 Cappellaro, E., Patat, F., Mazzali, P. A., et al. 2001, *ApJ*, 549, L215  
 Chandler, C. J., & Marvil, J. 2014, *ATel*, 5812  
 Chomiuk, L., Soderberg, A. M., Moe, M., et al. 2012, *ApJ*, 750, 164  
 de Vaucouleurs, G., de Vaucouleurs, A., Corwin, H. G., Jr., et al. 1991, *Third Reference Catalogue of Bright Galaxies* (New York: Springer)  
 Diehl, R., Siebert, T., Hillebrandt, W., et al. 2014, *Science*, 345, 1162  
 Dilday, B., Howell, D. A., Cenko, S. B., et al. 2012, *Science*, 337, 942  
 Di Stefano, R., Voss, R., & Claves, J. S. W. 2011, *ApJ*, 738, L1  
 Foley, R. J., Fox, O. D., McCully, C., et al. 2014, *MNRAS*, 443, 2887  
 Gall, E. E. E., Taubenberger, S., Kromer, M., Sim, S. A., Benetti, S., Blanc, G., Elias-Rosa, N., & Hillebrandt, W. 2012, *MNRAS*, 427, 994  
 Garnavich, P. M., Kirshner, R. P., Challis, P., et al. 2001, *BAAS*, 33, 1370  
 Goobar, A., Johansson, J., Amanullah, R., et al. 2014a, *ApJ*, 784, L12  
 Goobar, A., Kromer, M., Siverd, R., et al. 2014b, *ApJ*, in press  
 Goobar, A., & Leibundgut, B. 2011, *Annual Review of Nuclear and Particle Science*, 61, 251  
 Graham, M. L., Foley, W., Zheng, W., et al. 2015, *MNRAS*, 446, 2073  
 Graham, M. L., Valenti, S., Fulton, B. J., et al. 2014, *ApJ*, submitted [arXiv:1412.0653]  
 Hachisu, I., Kato, M., Saio, H., & Nomoto, K. 2012, *ApJ*, 744, 69  
 Hancock, P. J., Gaensler, B. M., & Murphy, T. 2011, *ApJ*, 735, 35  
 Hughes, J. P., Chugai, N., Chevalier, R., Lundqvist, P., & Schlegel, E. 2007, *ApJ*, 670, 1260  
 Iben, Jr., I., & Tutukov, A. V. 1984, *ApJS*, 54, 335  
 Ivanova, N., & Taam, R. E. 2004, *ApJ*, 601, 1058  
 Jerkstrand, A., Fransson, C., & Kozma, C. 2011, *A&A*, 535, 45  
 Johansson, J., Goobar, A., Kasliwal, M. M., et al. 2014, submitted to *MNRAS* [arXiv:1411.3322]  
 Justham, S. 2011, *ApJ*, 730, L34  
 Kasen, D. 2010, *ApJ*, 708, 1025  
 Kawabata, K. S., Akitaya, H., Yamanaka, M., et al. 2014, *ApJ*, 795, L4  
 Kelly, P. L., Fox, O. D., Filippenko, A. V., et al. 2014, *ApJ*, 790, 3  
 Kozma, C., Fransson, C., Hillebrandt, W., et al. 2005, *A&A*, 437, 983  
 Leonard, D. C. 2007, *ApJ*, 670, 1275  
 Levanon, N., Soker, N., & García-Berro, E. 2014, *MNRAS*, in press [arXiv:1408.1375]  
 Li, W., Bloom, J. S., Podsiadlowski, P., et al. 2011, *Nature*, 480, 348  
 Liu, Z. W., Kromer, M., Fink, M., et al. 2013a, *ApJ*, 778, 121  
 Liu, Z. W., Pakmor, R., Röpke, F. K., et al. 2012, *A&A*, 548, A2  
 Liu, Z. W., Pakmor, R., Seitenzahl, I. R., et al. 2013b, *ApJ*, 774, 37  
 Lundqvist, P., Mattila, S., Sollerman, J., et al. 2013, *MNRAS*, 435, 329  
 Maeda, K., Benetti, S., Stritzinger, M., et al. 2010a, *Nature*, 466, 82  
 Maeda, K., Kutsuna, M., & Shigeyama, T. 2014, *ApJ*, 794, 37  
 Maeda, K., Taubenberger, S., Sollerman, J., Mazzali, P. A., Leloudas, G., Nomoto, K., & Motohara, K. 2010b, *ApJ*, 708, 1703  
 Maoz, D., Mannucci, F., & Nelemans, G. 2014, *ARA&A*, 52, 107  
 Margutti, R., Parrent, J., Kamble, A., et al. 2014, *ApJ*, 790, 52  
 Margutti, R., Soderberg, A. M., Chomiuk, L., et al. 2012, *ApJ*, 751, 134  
 Marietta, E., Burrows, A., & Fryxell, B. 2000, *ApJS*, 128, 615  
 Marion, G. H., Sand, D. J., Hsiao, E. Y., et al. 2015, *ApJ*, 798, 39  
 Mattila, S., Lundqvist, P., Sollerman, J., et al. 2005, *A&A*, 443, 649  
 McClelland, C. M., Garnavich, P. M., Milne, P. A., Shappee, B. J., & Pogge, R. W. 2013, *ApJ*, 767, 119  
 Minkowski, R. 1939, *ApJ*, 89, 156  
 Munari, U., Henden, A., Belligoli, R., et al. 2013, *New Astronomy*, 20, 30  
 Nomoto, K. 1982, *ApJ*, 253, 798  
 Nomoto, K., Thielemann, F.-K., & Yokoi, K. 1984, *ApJ*, 286, 644  
 Nugent, P., et al. 2011, *Nature*, 480, 340  
 Pakmor, R., Röpke, F. K., Weiss, A., & Hillebrandt, W. 2008, *A&A*, 489, 983  
 Pan, K.-C., Ricker, P. M., & Taam, R. E. 2012, *ApJ*, 750, 151  
 Panagia, N., Van Dyk, S. D., Weiler, K. W., et al. 2006, *ApJ*, 646, 369  
 Pan, K.-C., Ricker, P. M., & Taam, R. E. 2012, *ApJ*, 750, 151  
 Parrent J. T., Howell, D. A., Friesen, B., et al., 2012, *ApJ*, 752, L26  
 Patat, N., Benetti, S., Justham, S., et al. 2007a, *A&A*, 474, 931

- Patat, N., Chandra, P., Chevalier, R., et al. 2007b, *Science*, 317, 924
- Pérez-Torres, M. A., Lundqvist, P., Beswick, R. J., et al. 2014, *ApJ*, 792, 38
- Perlmutter, S., Aldering, G., Goldhaber, G., et al. 1999, *ApJ*, 517, 565
- Pogge, R. W., Atwood, B., Brewer, D. F., et al. 2010, *Proc. SPIE*, 7735, 77350A
- Press, W. H., Teukolsky, S. A., Vetterling, W. T., & Flannery, B. P. (ed.) 1992, *Numerical Recipes in C. The Art of Scientific Computing* (2nd ed.; Cambridge: Cambridge Univ. Press)
- Riess, A., Filippenko, A. V., Challis, P., et al., 1998, *AJ*, 116, 1009
- Rice, J. A. 2007, *Mathematical Statistics and Data Analysis* (3rd ed.; Duxbury, Thomson Brooks/Cole)
- Russell, B. R., & Immler, S. 2012, *ApJ*, 748, L29
- Shappee, B. J., Stanek, K. Z., Pogge, R. W., & Garnavich, P. M. 2013, *ApJ*, 762, L5
- Shen, K. J., Guillochon, J., & Foley, R. J. 2013, *ApJ*, 770, L35
- Silverman, J. M., Vinko, J., Kasliwal, M. M., et al. 2013, *MNRAS*, 436, 1225
- Simon, J. D., Gal-Yam, A., Gnat, O., et al. 2009, *ApJ*, 702, 1157
- Sollerman, J., Lindahl, J., Kozma, C., et al. 2004, *A&A*, 428, 555
- Sternberg, A., Gal-Yam, A., Simon, J. D., et al. 2014, *MNRAS*, 443, 1849
- Taubenberger, S., Elias-Rosa, N., Kerzendorf, W. E., et al. 2014, *MNRAS*, in press [arXiv:1411.7599]
- Taubenberger, S., Kromer, M., Pakmor, R., et al. 2013, *ApJ*, 775, L43
- Thielemann, F.-K., Nomoto, K., & Yokoi, K. 1986, *A&A*, 158, 17
- Torres, G. 2010, *AJ*, 140, 1158
- Wang, B., Meng, X., Chen, X., & Han, Z. 2009, *MNRAS*, 395, 847
- Wang, X., Wang, L., Filippenko, A., et al. 2012, *ApJ*, 749, 126
- Webbink, R. F. 1984, *ApJ*, 277, 355
- Whelan, J., & Iben, I. J. 1973, *ApJ*, 186, 1007
- Zheng, W., Shivvers, I., Filippenko, A. V., et al. 2014, *ApJ*, 783, L24